BIOCHEMISTRY
including biophysical chemistry & molecular biology

Article

pubs.acs.org/biochemistry

Multiple Locations of Peptides in the Hydrocarbon Core of Gel-Phase Membranes Revealed by Peptide ^{13}C to Lipid ^{2}H Rotational-Echo Double-Resonance Solid-State Nuclear Magnetic Resonance

Li Xie, Lihui Jia, Shuang Liang, and David P. Weliky*

Department of Chemistry, Michigan State University, East Lansing, Michigan 48824, United States

Supporting Information

ABSTRACT: Membrane locations of peptides and proteins are often critical to their functions. Solid-state rotational-echo double-resonance (REDOR) nuclear magnetic resonance is applied to probe the locations of two peptides via peptide ^{13}CO to lipid ^{2}H distance measurements. The peptides are KALP, an α-helical membrane-spanning peptide, and HFP, the β-sheet N-terminal fusion peptide of the HIV gp41 fusion protein that plays an important role in HIV−host cell membrane fusion. Both peptides are shown to have at least two distinct locations within the hydrocarbon core of gel-phase membranes. The multiple locations are attributed to snorkeling of lysine side chains for KALP and to the distribution of antiparallel β-sheet registries for HFP. The relative population of each location is also quantitated. To the best of our knowledge, this is the first clear experimental support of multiple peptide locations within the membrane hydrocarbon core. These data are for gel-phase membranes, but the approach should work for liquid-ordered membranes containing cholesterol and may be applicable to liquid-disordered membranes with appropriate additional analysis to take into account protein and lipid motion. This paper also describes the methodological development of $^{13}CO-^{2}H$ REDOR using the lyophilized I4 peptide that is α-helical and ^{13}CO-labeled at A9 and $^{2}H_{\alpha}$-labeled at A8. The I4 spins are well-approximated as an ensemble of isolated $^{13}CO-^{2}H$ spin pairs each separated by 5.0 Å with a 37 Hz dipolar coupling. A pulse sequence with rectangular 100 kHz ^{2}H π pulses results in rapid and extensive buildup of REDOR ($\Delta S/S_0$) with a dephasing time (τ). The buildup is well-fit by a simple exponential function with a rate of 24 Hz and an extent close to 1. These parameter values reflect nonradiative transitions between the ^{2}H spin states during the dephasing period. Each spin pair spends approximately two-thirds of its time in the $^{13}CO-^{2}H$ ($m = \pm 1$) states and approximately one-third of its time in the $^{13}CO-^{2}H$ ($m = 0$) state and contributes to the $\Delta S/S_0$ buildup during the former but not the latter time segments.

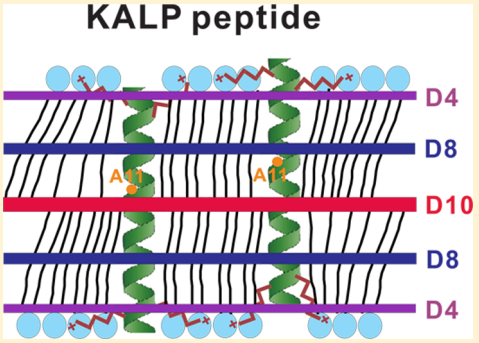

Residue-specific membrane locations are an important feature of membrane-bound peptides and proteins and in some cases are correlated with function.[1,2] These locations have been semiquantitatively probed by relaxation-based approaches, including fluorescence, electron paramagnetic resonance (EPR), and solid-state nuclear magnetic resonance (SSNMR).[3−8] More quantitative locations have been based on SSNMR measurements of peptide-to-lipid internuclear distances. For example, the proximity to the lipid headgroups has been probed via rotational-echo double-resonance (REDOR) determination of peptide backbone ^{13}CO to lipid ^{31}P internuclear distances.[2,9] Locations within the membrane hydrocarbon core have been probed by $^{13}CO-^{19}F$ REDOR of samples with ∼0.1 mole fraction of lipids with selective $^{1}H \rightarrow {}^{19}F$ substitutions in their acyl chains.[1,9] A $^{1}H \rightarrow {}^{19}F$ substitution is a chemical change and has the potential disadvantage of changing acyl chain and/or peptide location within the membrane.[10] A better approach is $^{13}CO-^{2}H$ REDOR of samples with lipids with $^{1}H \rightarrow {}^{2}H$ substitutions in their acyl chains. ^{1}H and ^{2}H are chemically equivalent, so there is no perturbation of the acyl chain or peptide locations.[11−15]

It is typical to develop a model with a single membrane location of the peptide based on data from the previously described approaches and the known peptide structure. It is atypical to consider a quantitative model with a distribution of membrane locations (e.g., multiple distinct locations with different populations), in part because the effects of this distribution on the data cannot be readily deconvolved from other effects. For example, even for a single membrane location, there is a broad distribution of peptide ^{13}C to lipid ^{19}F distances because the samples contain only a small fraction of fluorinated lipids.[9] To the best of our knowledge, this study describes the first clear experimental support for a distribution of membrane locations of a peptide within the hydrocarbon core and relies on peptide ^{13}CO to lipid ^{2}H distances of samples with large (≥0.8) mole fractions of deuterated lipids, which minimizes the intrinsic distribution of $^{13}CO-^{2}H$ distances. The experimental results of this study are compared to recent molecular dynamics

Received: September 25, 2014
Revised: December 19, 2014
Published: December 22, 2014

DOI: 10.1021/bi501211x
Biochemistry 2015, 54, 677−684

simulations of the distribution of membrane locations of a transmembrane helix. This study was conducted with gel-phase membranes lacking cholesterol, but the approach should be readily applicable to liquid-ordered-phase membranes containing cholesterol. The approach may also be applicable to fluid-phase membranes lacking cholesterol with additional analysis to take into account peptide and lipid motion.

The $^{13}CO-^{2}H$ REDOR experiment and analysis are developed and validated using the 17-residue I4 peptide that is lyophilized and has a regular α-helical structure.[16,17] I4 is synthesized with a specific ^{13}CO label at A9 and $^{2}H_{\alpha}$ label at A8. To a good approximation, the sample has isolated $^{13}CO-^{2}H$ spin pairs that all have the same internuclear separation (r) of 5.0 Å with a corresponding dipolar coupling (d) of 37 Hz.

MATERIALS AND METHODS

Peptides and Lipids. The $^{13}CO-^{2}H$ REDOR experiment and analysis were developed using the lyophilized I4_A9$_C$ peptide that has predominant α-helical structure (sequence of AEAAAKEAAAKEAAAKAW) and A8 $^{2}H_{\alpha}$ and A9 ^{13}CO labels separated by 5.0 Å (Table 1).[16,17] The membrane-associated

Table 1. Peptide Sequences

peptide	sequence[a]
I4_A9$_C$	AEAAAKEA**A**AKEAAAKAW
KALP_A11$_C$	GKKLALAL**A**LALALALALKKA
HFP_G5$_C$	AVGI**G**ALFLGFLGAAGSTMGARSWKKKKKKA
HFP_F8$_C$	AVGIGAL**F**LGFLGAAGSTMGARSWKKKKKKA

[a]An underlined residue has a backbone ^{13}CO label, and a bold residue has a $^{2}H_{\alpha}$ label.

peptides were (1) KALP_A11$_C$ (sequence of GKKLALALALALALALALKKA and A11 ^{13}CO label) and (2) HFP_G5$_C$ and HFP_F8$_C$ (sequence of AVGIGALFLGFLGAAGSTMGARSWKKKKKKA and either G5 or F8 ^{13}CO labels). KALP is a designed transmembrane peptide with α-helical structure, and HFP contains the N-terminal fusion peptide of the HIV gp41 protein.[1,18] HFP plays a key role in gp41-catalyzed fusion between the HIV and host cell membranes. HFP has oligomeric antiparallel β-sheet structure.[19,20] Membranes contained dipalmitoylphosphatidylcholine (DPPC) lipid deuterated at palmitoyl carbons 2 (D4), 7 and 8 (D8), or 15 and 16 (D10), or dimyristoylphosphatidylcholine (DMPC) perdeuterated at myristoyl carbons 2–14 (D54) (Figure 1). The D4 ^{2}H's are close to the membrane headgroups, and the D8 and D10 ^{2}H's are at the leaflet midpoint and bilayer center, respectively (Figures 3C and 4E,F). The DPPC and DMPC data are directly comparable because of very similar chemical structures. The HFP_G5$_C$ samples also included 0.2 mole fraction DTPG (ditetradecylphosphatidylglycerol) lipid, which reflects some negatively charged lipids in host cell membranes.[21]

Peptides were made by Fmoc solid-phase peptide synthesis and purified by reversed-phase high-performance liquid chromatography using a C4 column. The purity was >95% as assessed by mass spectrometry. I4 and KALP had N-terminal acetylation, and KALP also had C-terminal amidation. Lipids were purchased from Avanti Polar Lipids (Alabaster, AL) and synthesized using deuterated carboxylic acids purchased from CDN Isotopes (Pointe Claire, QC).

Sample Preparation. The I4 sample was lyophilized peptide without lipid. The other samples contained 50 μmol

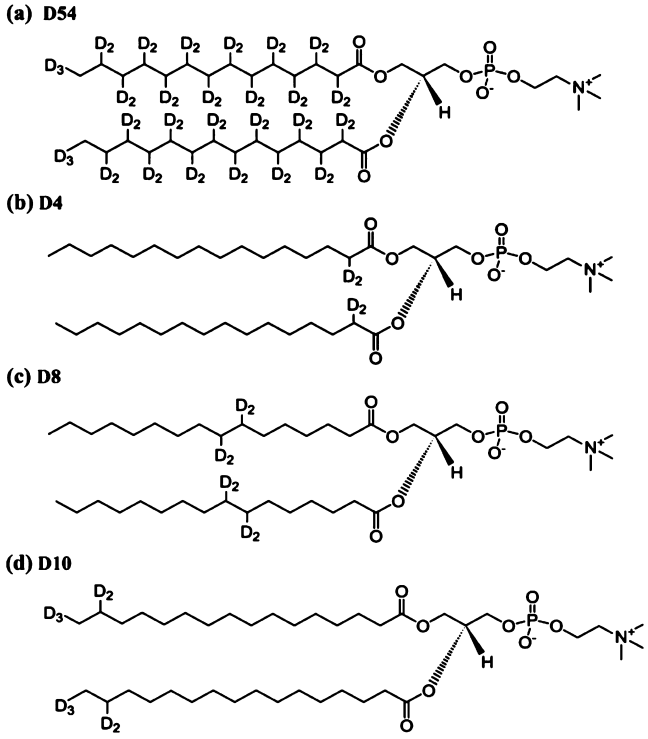

Figure 1. Chemical structures and ^{2}H labeling of the lipids.

of lipid and either 1 μmol of KALP or 2 μmol of HFP. Lipid and peptide were dissolved in a 2:3:2 volume ratio mixture of 2,2,2-trifluoroethanol, chloroform, and 1,1,1,3,3,3-hexafluoroisopropanol. Cosolubilization minimized the fraction of kinetically trapped peptide on the membrane surface. Solvent was removed by nitrogen gas and overnight vacuum. The peptide/lipid film was then suspended in 5 mM HEPES/10 mM MES buffer (pH 7.4) and homogenized by 10 freeze/thaw cycles in liquid nitrogen. After centrifugation at 270000g for 4 h, the harvested pellet was lyophilized, packed in a 4 mm diameter magic angle spinning (MAS) rotor, and hydrated with 20 μL of buffer.

Solid-State NMR Spectroscopy and Data Analysis. Data were acquired with a 9.4 T spectrometer and a triple-resonance probe tuned to ^{1}H, ^{13}C, and ^{2}H frequencies. Samples were cooled with gaseous nitrogen at −50 °C, which corresponded to a sample temperature of approximately −30 °C. The magic angle spinning (MAS) frequency is 10.00 kHz, and the pulse sequence is as follows: (1) ^{1}H $\pi/2$ pulse, (2) $^{1}H-^{13}C$ cross-polarization (CP), (3) dephasing period of duration τ, and (4) ^{13}C detection (Figure S1 of the Supporting Information). S_0 and S_1 acquisitions did not and did have, respectively, ^{2}H π pulses in the middle of each rotor cycle during the dephasing period. Both acquisitions had ^{13}C π pulses at the end of each rotor cycle during the dephasing period (except the last one) as well as ^{1}H decoupling during the dephasing and detection periods. Parameters included (1) a 5.0 μs ^{1}H $\pi/2$ pulse, (2) a 1.5 ms CP with 50 kHz ^{1}H and 62–66 kHz ramped ^{13}C fields, (3) 8.3 μs ^{13}C π pulses and 5.1 μs ^{2}H π pulses, and (4) 75 kHz ^{1}H decoupling with two-pulse phase modulation. The recycle delay was 1 s for τ values of 2, 8, and 16 ms, 1.5 s for τ values of 24 and 32 ms, and 2 s for τ values of 40 and 48 ms. Spectra were processed with 100 Hz Gaussian line broadening and baseline correction and externally referenced to the methylene peak of adamantane at 40.5 ppm.[22]

DOI: 10.1021/bi501211x
Biochemistry 2015, 54, 677–684

The experimental $(\Delta S/S_0)^{exp} = (S_0 - S_1)/S_0$ values at each τ were calculated using S_0 and S_1 ^{13}CO intensities determined with a 3.0 ppm integration window. The uncertainty of the S_0 or S_1 intensities (σ) is determined as the standard deviation of the experimental intensities from spectral regions that do not contain signal. The 3 ppm integration window in each region matches that used for S_0 and S_1 integration. The uncertainty in $\Delta S/S_0$ is calculated from propagation of error as $\sigma[(1/S_0)^2 + (S_1/S_0^2)^2]^{1/2}$. For the I4 peptide, similar dephasing was observed with 6, 8, and 10 kHz MAS frequencies; e.g., for the 24 ms dephasing time, the respective $(\Delta S/S_0)^{exp}$ values were 0.38(3), 0.40(1), and 0.38(1), respectively.

Comparison was made between the $(\Delta S/S_0)^{exp}$ of the I4 sample and the $(\Delta S/S_0)^{sim}$ calculated for isolated $^{13}CO-^2H$ spin pairs using the SIMPSON simulation program.[23] Inputs to the program include the rf fields of the pulses, the MAS frequency, and the ^2H quadrupolar anisotropy. The program was also used to calculate the contribution of natural abundance (na) ^{13}CO nuclei to the $(\Delta S/S_0)^{exp}$ of the I4 sample and then determine the $(\Delta S/S_0)^{lab}$ associated with the labeled (lab) A9 ^{13}CO nuclei. The $r_k \equiv {}^{13}CO_k{}^{na}-{}^2H_\alpha{}^{A8}$ separation was determined for each na $^{13}CO_k$ site using a model of regular α-helical structure. r_k was used to determine the corresponding $^{13}CO_k-^2H$ dipolar coupling d_k. The $(\Delta S/S_0)_k^{na}$ versus τ was calculated using the SIMPSON program with input d_k. The $(\Delta S/S_0)^{lab}$ was then calculated using

$$(\Delta S/S_0)^{exp} = f_{lab}(\Delta S/S_0)^{lab} + f_{na}(\Delta S/S_0)^{na} \quad (1)$$

where $(\Delta S/S_0)^{na} = \sum_k[(\Delta S/S_0)_k^{na}]/\sum_k$ and f_{lab} and f_{na} are the total fractional populations of lab and na ^{13}CO nuclei, respectively. The typical $(\Delta S/S_0)^{lab} \approx 1.08(\Delta S/S_0)^{exp}$ for the I4 peptide. Table S2 of the Supporting Information presents all $(\Delta S/S_0)^{exp}$ and $(\Delta S/S_0)^{lab}$ values versus τ.

For the membrane samples, semiquantitative understanding of the relative contributions of $(\Delta S/S_0)^{lab}$ and $(\Delta S/S_0)^{na}$ to $(\Delta S/S_0)^{exp}$ is obtained with a model for which half the na sites have r_k values similar to r_{lab} and half are more distant such that their $(\Delta S/S_0)_k^{na} \approx 0$. For this model, the average $(\Delta S/S_0)^{na} \approx (\Delta S/S_0)^{lab}/2$, and for $f_{lab} \approx 0.8$ and $f_{na} \approx 0.2$, the consequent $(\Delta S/S_0)^{lab} \approx 1.1(\Delta S/S_0)^{exp}$. Because the differences between the $(\Delta S/S_0)^{exp}$ and $(\Delta S/S_0)^{lab}$ values are small and somewhat uncertain, data analysis for the membrane samples is based on $(\Delta S/S_0)^{exp}$.

RESULTS

Representative S_0 (black) and S_1 (colored) spectra with a τ of 40 ms are displayed in the insets of Figures 2–4. For S_0 and S_1, there was respective complete and incomplete averaging of $^{13}CO-^2H$ dipolar coupling, with an S_1 ^{13}CO spectral intensity consequently smaller than that of S_0. The I4_A9$_C$ and KALP_A11$_C$ ^{13}CO peak shifts are 179 ppm and consistent with α-helical structure.[22,24] The HFP_F8$_C$ and HFP_G5$_C$ shifts are 174 and 171 ppm, respectively, and consistent with β-sheet structure.[19] The ^{13}CO S_0 intensities have ~0.8 fractional contribution from the labeled (lab) nuclei; e.g., for KALP, the lab signal = 0.99 and the natural abundance (na) signal = 0.24 (0.011 × 22). The experimental buildup $(\Delta S/S_0)^{exp} = (S_0 - S_1)/S_0$ versus τ is calculated from ^{13}CO S_0 and S_1 intensities. The experimental $(\Delta S/S_0)^{exp}$ values typically differ by at most 10% from the $(\Delta S/S_0)^{lab}$ values of the lab ^{13}CO nuclei as explained in Materials and Methods.

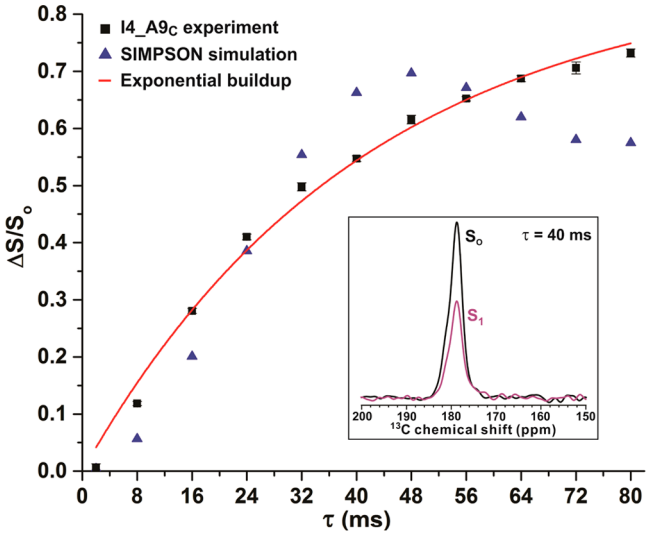

Figure 2. $^{13}CO-^2H$ REDOR spectra with a 40 ms dephasing time for the I4_A9$_C$ peptide as well as $\Delta S/S_0$ vs τ. Black squares are the $(\Delta S/S_0)^{lab}$ values of the labeled A9 ^{13}CO nuclei and are numerically very close to the experimental $(\Delta S/S_0)^{exp}$. For all values of τ, the difference between the $(\Delta S/S_0)^{lab}$ and $(\Delta S/S_0)^{exp}$ values is ≤0.06 (Table S2 of the Supporting Information). The uncertainties are displayed for all $(\Delta S/S_0)^{lab}$ data, but in many cases, the uncertainties are comparable to or smaller than the displayed black squares. Blue triangles are $(\Delta S/S_0)^{sim}$ calculated using the SIMPSON program without ^2H relaxation. The $(\Delta S/S_0)^{sim}$ values are best-fit to the $(\Delta S/S_0)^{lab}$ with a 22 Hz $^{13}CO-^2H$ dipolar coupling. The red line is the best-fit exponential buildup. The peptide is synthesized with a specific ^{13}CO label at A9 and a $^2H_\alpha$ label at A8. To a good approximation, the sample has isolated $^{13}CO-^2H$ spin pairs that all have the same internuclear separation (r) of 5.0 Å with a corresponding dipolar coupling (d) of 37 Hz. The sample contains ~15 μmol of lyophilized peptide. The number of summed S_0 or S_1 scans is 500 for τ values of 2–48 ms and 2000 for τ values of 56–80 ms.

The membrane samples were likely in the thermodynamic equilibrium state. This assertion was evidenced by $\Delta S/S_0$ values of replicate samples that agreed to within ±0.03. In addition, similar $\Delta S/S_0$ values were observed in a sample prepared using a different means of incorporation of peptide into the membrane, in particular: (1) mixing HFP_G5$_C$ with unilamellar lipid vesicles (D10+DTPG) in an aqueous solution, (2) centrifugation to form a pellet containing vesicles and bound HFP with unbound HFP in an aqueous solution, and (3) lyophilization of the pellet, packing in the rotor, and hydration with buffer. The $\Delta S/S_0$ of this sample agreed within ±0.05 with the $\Delta S/S_0$ of the comparable HFP_G5$_C$ sample prepared by organic cosolubilization.

Analysis of the REDOR Data of the I4_A9$_C$ Sample. This is an excellent model system because it contains isolated $^{13}CO-^2H$ spin pairs that have r = 5.0 Å and d = 37 Hz (Figure 2). The REDOR experiment was conducted with an ~100 kHz ^2H rf field, and the $(\Delta S/S_0)^{lab}$ buildup is rapid and extensive. This is generally consistent with buildups calculated using the SIMPSON quantum mechanics simulation program with ^2H fields of ≥100 kHz (Figure S3 of the Supporting Information). For ≤40 kHz fields, the calculated buildups are attenuated because of the ~65 kHz distribution of ^2H resonant offsets associated with a rigid $C-^2H$ bond. Attenuated buildups have been observed in previous experiments performed with lower ^2H rf fields.[15]

DOI: 10.1021/bi501211x
Biochemistry 2015, 54, 677–684

There are also systematic differences between $(\Delta S/S_0)^{lab}$ and the best-fit SIMPSON-calculated $(\Delta S/S_0)^{sim}$ of the I4_A9$_C$ sample, including respective exponential versus sigmoidal shapes and maximal values of ∼1 versus ∼(2/3). In addition, the best-fit d of 22 Hz is smaller than the expected d of 37 Hz. The differences are not due to deviation from regular α-helical structure. An earlier ^{13}CO−^{15}N REDOR study of the I4 peptide with A9 ^{13}CO and A13 ^{15}N labeling yielded a buildup of $(\Delta S/S_0)^{exp}$ versus τ that was very well-fit by SIMPSON to a 45 Hz coupling corresponding to the expected $^{13}CO_{A9}$−$^{15}N_{A13}$ distance of 4.1 Å in an α-helix.[17]

The differences for ^{13}CO−^{2}H REDOR between $(\Delta S/S_0)^{lab}$ and $(\Delta S/S_0)^{sim}$ are explained by effects of nonradiative transitions between the $m = \pm1$ states and the $m = 0$ states of individual ^{2}H nuclei during the dephasing period that are not considered in the SIMPSON calculations. These transitions are evidenced by measured ^{2}H T_1 relaxation times in our samples in the 50−100 ms range (Table S1 of the Supporting Information). As detailed below, there is an effect on $(\Delta S/S_0)^{lab}$ because these nonradiative transitions have a much greater effect on the S_1 signal than on the S_0 signal.

At any specific time during the dephasing period, the I4 sample has a two-thirds fractional population of ^{13}CO−^{2}H ($m = \pm1$) spin pairs that experience dipolar coupling and a one-third fractional population of ^{13}CO−^{2}H ($m = 0$) pairs that do not experience dipolar coupling. In the absence of ^{2}H relaxation, a spin pair is either ^{13}CO−^{2}H ($m = \pm1$) or ^{13}CO−^{2}H ($m = 0$) for the entire dephasing period. During each rotor cycle of the S_0 acquisition, the dipolar evolution of a ^{13}CO−^{2}H ($m = \pm1$) pair is completely refocused by MAS so the pair makes a full contribution to the ^{13}CO S_0 signal. Dipolar evolution is not refocused during a rotor cycle of the S_1 acquisition, and the pair makes an attenuated contribution to the S_1 signal. A ^{13}CO−^{2}H ($m = 0$) pair does not experience coupling, so there is not evolution for either the S_0 or S_1 acquisition and there are complete and equal contributions to the S_0 and S_1 signals. In the absence of relaxation, the $\Delta S/S_0$ buildup is therefore only due to ^{13}CO−^{2}H ($m = \pm1$) pairs, so the consequent $(\Delta S/S_0)_{max}$ is expected to be ∼(2/3). This is observed for the SIMPSON calculation that does not include relaxation (Figure 2).

In the presence of ^{2}H relaxation with T_1 comparable to the dephasing period, there may be one or a few instantaneous and stochastic changes in a ^{2}H m state. Stochastic means the transitions of individual ^{2}H's are uncorrelated with each other but there is a defined overall transition rate. For the S_0 acquisition, there is dipolar evolution for a ^{13}CO−^{2}H pair during the one or few S_0 rotor cycles in which the ^{2}H changes from $m = \pm1$ to $m = 0$ or vice versa. However, the net S_0 signal attenuation is negligible because there is no evolution during the other (typically hundreds of) rotor cycles of the dephasing period.

Relaxation has a larger impact on the S_1 signal. A spin pair is ^{13}CO−^{2}H ($m = \pm1$) during some time segments of the dephasing period and ^{13}CO−^{2}H ($m = 0$) during other segments. There is dipolar evolution during the ^{13}CO−^{2}H ($m = \pm1$) segments with a corresponding attenuated contribution to the S_1 signal and no evolution during the ^{13}CO−^{2}H ($m = 0$) segments and corresponding full contribution to the S_1 signal. As noted above, the $m = \pm1 \leftrightarrow m = 0$ transitions are stochastic, so the time segments are uncorrelated among the ^{2}H nuclei. Qualitatively, each pair spends approximately two-thirds of the dephasing period as ^{13}CO−^{2}H ($m = \pm1$) and approximately one-third as ^{13}CO−^{2}H ($m = 0$). It is therefore expected that the buildup rate of $\Delta S/S_0$ will be ∼(2/3) the dipolar coupling for ^{13}CO−^{2}H ($m = \pm1$) pairs. This matches the fitting of the I4 data with SIMPSON calculations. The best-fit d = 22 Hz is ∼(2/3) of the known d = 37 Hz of the ^{13}CO−^{2}H ($m = \pm1$) pairs of this sample.

Relaxation also affects the value of $(\Delta S/S_0)_{max}$. Most pairs are ^{13}CO−^{2}H ($m = \pm1$) for some segments of the dephasing period and therefore contribute to the $\Delta S/S_0$ buildup. The $\Delta S/S_0$ for large τ values is therefore expected to be >(2/3), which is consistent with the $\Delta S/S_0$ of Figure 2.

The SIMPSON program is based on coherent quantum mechanics, and it is not straightforward to incorporate stochastic changes of the ^{2}H m state into this program. Analysis of $(\Delta S/S_0)^{exp}$ versus τ is instead based on excellent fitting to the simple exponential buildup function $A(1 - e^{-\gamma\tau})$, where γ and A are fitting parameters (Figures 2−4 and Table 2). The buildup rate γ is correlated to the ^{13}CO−^{2}H dipolar coupling, and the buildup extent A is correlated to the fraction of lab ^{13}CO nuclei with this coupling. The corresponding value of $1 - A$ is correlated to the fraction of lab ^{13}CO nuclei not coupled to ^{2}H. These correlations are most quantitatively understood from the fitting results for the I4 sample that contains isolated ^{13}CO−^{2}H spin pairs with r = 5.0 Å and corresponding d = 37 Hz. The best-fit γ = 24 Hz ≈ $(2/3)d$ is consistent with an individual ^{2}H spending approximately two-thirds of the dephasing period in the $m = \pm1$ states and approximately one-third in the $m = 0$ state. For this model of ^{2}H relaxation, all ^{13}CO−^{2}H pairs contribute to the $\Delta S/S_0$ buildup, and the expected $(\Delta S/S_0)_{max} \approx 1$. However, the best-fit A = 0.87 implies that 0.13 fraction of the pairs remain as ^{13}CO−^{2}H ($m = 0$) for the longest measured dephasing period.

Table 2. REDOR Fitted Parameters[a]

sample	A	γ (Hz)	d (Hz)	r (Å)
I4_A9$_C$	0.87(5)	24(2)	37	5.0
KALP_A11$_C$ in D8	0.15(2)	47(10)	72(15)	4.0(3)
KALP_A11$_C$ in D10	0.48(4)	34(5)	52(8)	4.5(2)
KALP_A11$_C$ in D54	0.96(1)	85(4)	131(6)	3.3(1)
HFP_F8$_C$ in D8	0.21(1)	71(10)	109(15)	3.5(2)
HFP_F8$_C$ in D10	0.82(20)	16(5)	25(8)	5.7(6)
HFP_F8$_C$ in D54	0.99(1)	122(1)	188(2)	2.9(1)
HFP_G5$_C$ in D8 with DTPG	0.45(5)	27(5)	42(8)	4.8(3)
HFP_G5$_C$ in D10 with DTPG	0.85(3)	37(3)	57(5)	4.3(1)

[a]The fitting function is $A(1 - e^{-\gamma\tau})$. The $\gamma = 0.65d$ is determined from the known ^{13}CO−^{2}H dipolar coupling d = 37 Hz for the I4 sample. This correlates to $\gamma = (2/3)d$ expected when a ^{2}H spin spends approximately equal times during the dephasing period in the $m = \pm1$ and $m = 0$ states because of $m = \pm1 \leftrightarrow m = 0$ nonradiative transitions. The calculated ^{13}CO−^{2}H distance $r = (4642/d)^{1/3}$ is quantitative for a sample like I4 that contains isolated ^{13}CO−^{2}H spin pairs with a single separation. For the KALP and HFP samples, a ^{13}CO may be coupled to multiple ^{2}H's, although the buildup rate γ is probably dominated by coupling to the closest ^{2}H. The small r values of the perdeuterated D54 samples are closer than the expected ^{13}CO−^{2}H van der Waals separation and may reflect couplings to multiple nearby ^{2}H's. The fitted A is correlated to the fraction of molecules with the fitted γ and corollary-calculated d and r. The term $1 - A$ is correlated to the fraction of molecules with $d \approx 0$. The $A_{D8} + A_{D10} > 1$ of HFP_G5$_C$ may mean that some G5 ^{13}CO nuclei contact both D8 and D10 ^{2}H nuclei.

DOI: 10.1021/bi501211x
Biochemistry 2015, 54, 677−684

This fraction matches the expected value for $\tau \approx T_1$, as calculated using $(1/3)(1 - e^{-\tau/T_1})$.

We do not have a rigorous argument to explain the observation of exponential buildup of $\Delta S/S_0$ versus τ. However, stochastic processes often lead to exponential time dependence, e.g., NMR longitudinal and transverse relaxation.

KALP and HFP. Membrane locations of peptides are assessed by comparative analysis of the $(\Delta S/S_0)^{exp}$ with lipids with perdeuterated (D54) or selectively deuterated (D4, D8, or D10) acyl chains (Figures 3 and 4). In the absence of ^{2}H relaxation, sigmoidal buildups are expected. However, like I4, all

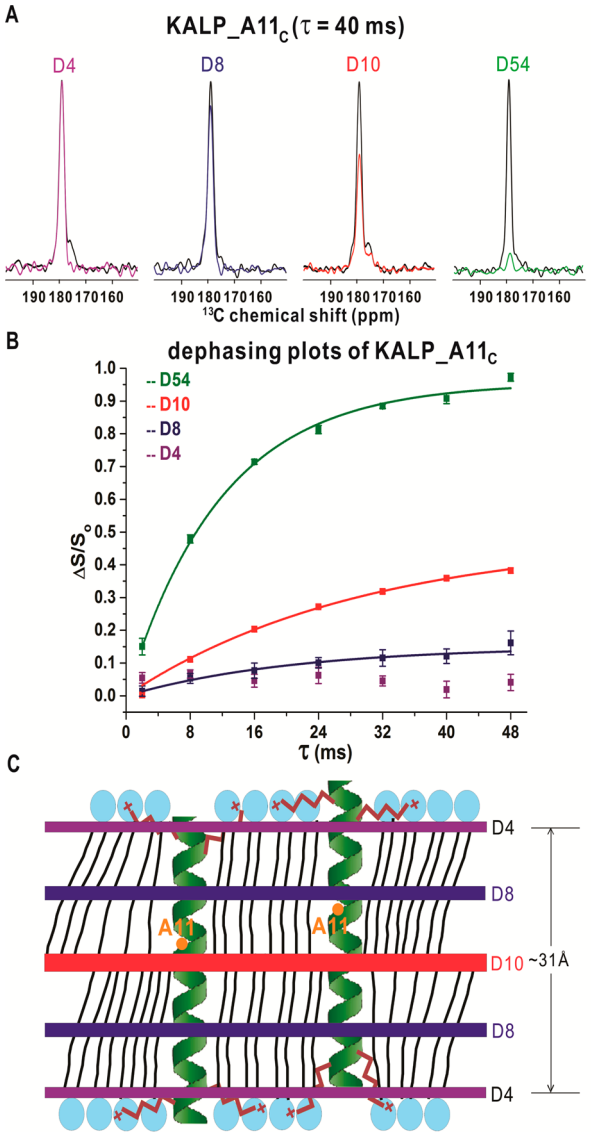

Figure 3. (A) τ = 40 ms S_0 (black) and S_1 (colored) ^{13}CO−^{2}H REDOR spectra of KALP_A11$_C$. (B) Experimental $(\Delta S/S_0)^{exp}$ (points with uncertainties) and best-fit exponential buildup (solid line) plots of $\Delta S/S_0$ vs τ. The D4 data are not fit. The uncertainties are displayed for all $(\Delta S/S_0)^{exp}$ data, but in many cases, the uncertainties are comparable to or smaller than the displayed symbols. (C) Membrane locations of KALP with major (left) and minor (right) populations. The colored bands are ^{2}H positions; the A11 ^{13}CO nuclei are orange dots, and the lysine side chains are brown lines. The samples contain ~1 μmol of peptide and ~50 μmol of lipid. For the displayed τ = 40 ms spectra, the numbers of summed S_0 or S_1 scans are 18165 for D4, 31416 for D8, 25998 for D10, and 26882 for D54.

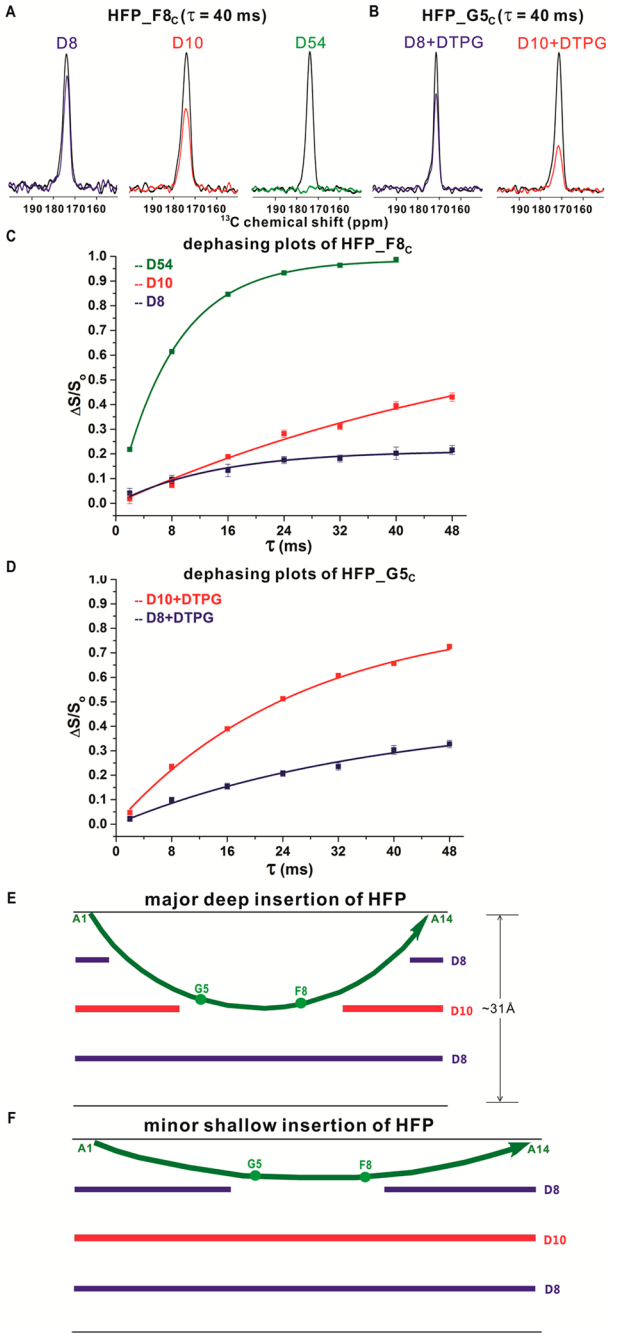

Figure 4. τ = 40 ms S_0 (black) and S_1 (colored) ^{13}CO−^{2}H REDOR spectra of membrane-associated (A) HFP_F8$_C$ and (B) HFP_G5$_C$. Experimental $(\Delta S/S_0)^{exp}$ (points with uncertainties) and best-fit exponential buildup (solid line) plots of $\Delta S/S_0$ vs τ of (C) HFP_F8$_C$ and (D) HFP_G5$_C$. The uncertainties are displayed for all $(\Delta S/S_0)^{exp}$ data, but in many cases, the uncertainties are comparable to or smaller than the displayed black squares. (E and F) Deep and shallow membrane insertion of HFP. Residues A1 and A14 are close to the membrane surface in concurrence with peptide ^{13}CO−lipid ^{31}P distances of ~5 Å for these residues.[1] For the sake of clarity, only one β-strand is displayed. The samples contain ~2 μmol of peptide and ~50 μmol of lipid. For the displayed τ = 40 ms spectra of the HFP_F8$_C$ samples, the numbers of summed S_0 or S_1 scans are 21799 for D8, 38797 for D10, and 14113 for D54. For the displayed HFP_G5$_C$ spectra, the numbers are 34727 for D8 with DTPG and 35602 for D10 with DTPG.

DOI: 10.1021/bi501211x
Biochemistry 2015, 54, 677−684

membrane peptide data are well-fit by single-exponential but not sigmoidal buildups (Table 2). This is consistent with a ^{2}H relaxation effect that is additionally evidenced by measured T_1's typically in the range of 50−100 ms (Table S1 of the Supporting Information). Each fitted γ is interpreted with a single ^{13}CO−^{2}H spin pair model with calculated $d = \gamma/0.65$ and r (Å) = $[4642/d\ (\text{Hz})]^{1/3}$. The $(\Delta S/S_0)^{\text{exp}}$ values reflect coupling of peptide ^{13}CO to multiple lipid ^{2}H's. However, because of the r^{-3} dependence of coupling, the buildup rates for the D4, D8, and D10 samples are likely dominated by the closest pair. This is supported by r values of ≈4−5 Å that match the peptide ^{13}CO−lipid ^{2}H van der Waals separation. The perdeuterated D54 samples likely have at least two close ^{2}H's, which results in buildup that is faster than that for a single ^{2}H. This is consistent with a calculated r of ≈3 Å, which is smaller than the van der Waals separation.

For either KALP or HFP, the D54 $(\Delta S/S_0)^{\text{exp}} \approx 1$ at longer values of τ results in best-fit $A \approx 1$. This supports the locations of A11 and F8 within the membrane hydrocarbon core for all KALP and HFP molecules. Rapid and quantitative $(\Delta S/S_0)^{\text{exp}}$ buildup also supports monomer rather than oligomer KALP because ^{13}CO's in the oligomer interior are distant from lipid ^{2}H's and would have slower buildup. Previous work showed oligomeric antiparallel β-sheet HFP. The rapid and quantitative HFP buildup supports small (∼10 molecule) oligomers in which all HFP molecules contact lipid acyl chains.

The D4, D8, and D10 data provide more detailed location information. One potential concern is that variation among buildup extents, i.e., A values, is primarily due to differences in ^{2}H quadrupolar anisotropies (characterized by the Pake doublet splitting $\Delta\nu_Q$) with smaller A values correlated to greater $\Delta\nu_Q$ values via the ^{2}H pulse resonance offset. However, this concern is not supported by several lines of evidence. The samples are cooled with N_2 gas at −50 °C, and the ^{2}H's have rigid $\Delta\nu_Q \approx$ 120 kHz with D4 and D8 and a superposition of $-CD_2$ $\Delta\nu_Q \approx$ 120 kHz and $-CD_3$ $\Delta\nu_Q \approx$ 30 kHz with D10 (Figure S2 of the Supporting Information). I4 and D54 samples have dominant $\Delta\nu_Q \approx$ 120 kHz, yet their buildups and A values are larger than those of D10 samples with smaller average $\Delta\nu_Q$ values. In addition, other peptide buildups show $A_{D8} > A_{D10}$, $A_{D4} > A_{D8}$, or $A(\text{-CD,-CD}_2) > A(\text{-CD}_3)$ (Figures S5−S7 of the Supporting Information). SIMPSON simulations incorporating the experimental 100 kHz ^{2}H π pulses show superimposable buildups for a $\Delta\nu_Q$ of either 120 or 0 kHz (Figure S3A of the Supporting Information).

Both KALP and HFP show significant buildups in D10 and D8 but not D4 membranes (Figures 3 and 4 and Figure S4 of the Supporting Information). This is consistent with D54 data and supports an α-helical KALP monomer with transmembrane topology and a β-sheet HFP with insertion into the membrane hydrocarbon core. Typical fittings show $A_{D10} \neq A_{D8}$ with both A values being <1 and also r values of ≈4−5 Å, which correspond to peptide ^{13}CO−lipid ^{2}H van der Waals contacts (Table 2). These parameters are inconsistent with a single membrane location for which $A_{D10} \approx A_{D8} \approx 1$ and $r_{D10} \neq r_{D8}$ would be expected. For example, KALP centered in the membrane would be evidenced by $r_{D10} \approx 4$ Å and $r_{D8} \geq 8$ Å. The actual KALP parameters could be understood only using two distinct membrane locations with major and minor populations (Figure 3C and Figure S8 of the Supporting Information). These populations have A11 contact with the D10 and D8 ^{2}H nuclei, respectively, and the A11 ^{13}CO nuclei are 2−3 and 7−8 Å from the membrane center, respectively. One reason for multiple KALP locations may be a hydrophobic KALP length of ∼26 Å (L4−L20), which is shorter than the hydrophobic length of the DPPC membrane (∼31 Å).[25,26] The KALP hydrophobic length could be increased by "snorkeling" of lysine side chains to the headgroup region, and the different KALP locations may be correlated with different snorkeling geometries.[27,28] The two experimentally determined locations in Figure 3C differ by an ∼5 Å translation along the membrane normal, which is comparable to the ∼8 Å range in molecular dynamics simulations for transmembrane helices.[8,29] KALP likely has additional membrane locations because the sum $A_{D8} + A_{D10} < 1$.

For either HFP_F8$_C$ or HFP_G5$_C$, there are very different values of A_{D10} and A_{D8}, and for HFP_G5$_C$, $r_{D8} \approx r_{D10} \approx 4.5$ Å. As with KALP, these trends support two distinct membrane locations of HFP. The larger A_{D10} values are attributed to a major HFP population with deep membrane insertion and HFP contact with D10 ^{2}H nuclei, and the smaller A_{D8} values are attributed to a minor population with shallow membrane insertion and HFP contact with D8 ^{2}H nuclei (Figure 4E,F). The major:minor population ratio is ∼7:3 as calculated from the τ = 48 ms $(\Delta S/S_0)_{D10}$-to-$(\Delta S/S_0)_{D8}$ ratio for either the HFP_F8$_C$ or HFP_G5$_C$ samples. The 7:3 ratio is also supported by the $\Delta S/S_0$ values at large τ values for HFP_G5$_C$ samples prepared with membranes with different deuterated cholesterols (Figure S7 of the Supporting Information). The A_{D10}/A_{D8} ratios are ∼4 for HFP_F8$_C$ and ∼2 for HFP_G5$_C$. However, there are ∼30% uncertainties in the best-fit A and γ values for the HFP_F8$_C$ (D10) sample, which are much larger than for other samples. The reason for these larger uncertainties is not well-understood, but it might be related to the use of neutral membrane in this sample rather than a membrane with a 0.2 fraction of negatively charged lipid as was used for the HFP_G5$_C$ samples. Relative to a neutral membrane, there is higher and more reproducible binding of the positively charged peptide to the negatively charged membrane, probably because of the contribution of the attractive electrostatic energy.

For HFP_G5$_C$, the relationship $A_{D8} + A_{D10} > 1$ may mean that some G5 ^{13}CO nuclei contact both D8 and D10 ^{2}H nuclei. There is negligible HFP localized to the membrane surface, as evidenced by $\Delta S/S_0 \approx 0$ for D4 samples (Figure S4 of the Supporting Information). The multiple membrane locations of HFP are attributed to the distribution of antiparallel β-sheet registries.[20] Specifically, the membrane insertion depth of a HFP registry likely depends on the lengths of its contiguous hydrophobic regions, and these lengths vary among registries. Deep and shallow insertions may also have a distribution of membrane locations of HFP. The predominant deep insertion of HFP could significantly perturb the membrane bilayer and lower the activation energy of membrane fusion. This is consistent with the observed strong positive correlation between membrane insertion depth and fusion rate for several HFP constructs.[1] Models in panels E and F of Figure 4 show insertion of the antiparallel β-sheet into a single leaflet rather than membrane traversal analogous to that of bacterial porins. The major deep insertion into a single leaflet is more consistent with the observed close contact of multiple HFP residues with the D10 ^{2}H's near the center of the membrane. Insertion into a single leaflet is also likely for the intermolecular β-sheet formed from multiple gp41 proteins during HIV−cell fusion.[30] This topology allows the other parts of all the ectodomains (∼160 residues per gp41) to be on the same face of the membrane.

DOI: 10.1021/bi501211x
Biochemistry 2015, 54, 677−684

DISCUSSION

$^{13}CO-^{2}H$ REDOR SSNMR reveals multiple locations within the hydrocarbon core of a gel-phase membrane for both the monomeric α-helical KALP peptide and the oligomeric β-sheet HFP peptide. The KALP locations are attributed to hydrophobic mismatch and consequent snorkeling of lysine side chains. The HFP locations are attributed to the distribution of antiparallel β-sheet registries. We consider whether multiple locations in gel-phase membranes that are derived from our data reflect multiple locations for peptides and proteins in cell membranes. One general difference between model and cell membranes is the higher ~1:1 (w/w) protein:lipid ratio of a typical cell membrane. The cell membrane also contains a mixture of distinct lipids and sterols specific to the cell type. HFP should be considered in the context of the membrane composition of host cells of HIV with a ~1:2 cholesterol:lipid mole ratio and ~50% PC and ~10% negatively charged lipid.[21] This composition is likely liquid-ordered phase, and in such membranes with significant cholesterol, the HFP HIV gp41 has β-sheet structure with a distribution of antiparallel registries.[20,31] There may be multiple locations for HFP in the cell membrane because of this distribution. KALP is a designed sequence, and there may be multiple membrane locations in higher-temperature single-component fluid-phase membranes because of hydrophobic mismatch. We note a recent study proposing two locations for a peptide in a fluid-phase membrane based on fluorescence and molecular dynamics simulations.[8]

We also consider future application of the protein ^{13}C membrane ^{2}H REDOR approach to probe the membrane locations of proteins. Experiments in liquid-ordered membranes containing cholesterol should be straightforward and could include detection of contacts between specific protein residues and specific cholesterol regions (Figure S7 of the Supporting Information). Experiments in fluid-phase membranes lacking cholesterol may be challenging because of motion by both the protein and the lipid. Such motion may result in reduced $^{13}CO-^{2}H$ dipolar coupling and a corresponding $\Delta S/S_0$ buildup rate via averaging of $\langle 3\cos^2\theta - 1\rangle$, where θ is the angle between the $^{13}CO-^{2}H$ internuclear vector and the external magnetic field. Even with motion, it should still be possible to distinguish the relative proximity of a residue to the D4, D8, and D10 deuterated regions, and a model transmembrane peptide like KALP could be used to validate the approach. $^{13}CO-^{2}H$ distances could be semiquantitatively derived using $\langle 3\cos^2\theta - 1\rangle$ values that are estimated from lipid order parameters and/or molecular dynamics simulations. The dipolar coupling and corresponding $\Delta S/S_0$ buildup typically have an only minor dependence on averaging of $\langle r^{-3}\rangle$. One practical change in the pulse sequence for obtaining higher signals for samples with motion may be use of an initial ^{13}C $\pi/2$ pulse rather than $^{1}H \rightarrow {}^{13}C$ cross-polarization.

Although our experiments were conducted with selectively labeled protein to allow unambiguous resonance assignment of one-dimensional spectra, the approach also can be applied to proteins with extensive ^{13}C and ^{15}N labeling with the caveat that the ^{13}C and ^{15}N line widths are narrow enough to allow resonance assignment via multidimensional SSNMR.[32] These experiments were also conducted with deuterated DPPC lipid because of the commercial availability of palmitic acid with different deuteration patterns. Future experiments could be conducted with more common biological lipids that contain a palmitoyl and an oleoyl chain. Experiments can also be conducted with deuterated cholesterol (Figure S7 of the Supporting Information).

ASSOCIATED CONTENT

Supporting Information

Additional SSNMR data and analysis. This material is available free of charge via the Internet at http://pubs.acs.org.

AUTHOR INFORMATION

Corresponding Author

*E-mail: weliky@chemistry.msu.edu. Phone: (517) 355-9715. Fax: (517) 353-1793.

Funding

This work was supported by National Institutes of Health Grant AI47153.

Notes

The authors declare no competing financial interest.

ABBREVIATIONS

d, dipolar coupling; D4, D8, and D10, deuterated dipalmitoylphosphatidylcholine lipids; D54, deuterated dimyristoylphosphatidylcholine lipid; DTPG, ditetradecylphosphatidylglycerol lipid; HFP, HIV fusion peptide; HIV, human immunodeficiency virus; MAS, magic angle spinning; *r*, $^{13}CO-^{2}H$ separation; REDOR, rotational-echo double-resonance; SSNMR, solid-state nuclear magnetic resonance.

REFERENCES

(1) Qiang, W., Sun, Y., and Weliky, D. P. (2009) A strong correlation between fusogenicity and membrane insertion depth of the HIV fusion peptide. *Proc. Natl. Acad. Sci. U.S.A. 106*, 15314−15319.

(2) Gabrys, C. M., Qiang, W., Sun, Y., Xie, L., Schmick, S. D., and Weliky, D. P. (2013) Solid-state nuclear magnetic resonance measurements of HIV fusion peptide ^{13}CO to lipid ^{31}P proximities support similar partially inserted membrane locations of the α helical and β sheet peptide structures. *J. Phys. Chem. A 117*, 9848−9859.

(3) Agirre, A., Flach, C., Goni, F. M., Mendelsohn, R., Valpuesta, J. M., Wu, F. J., and Nieva, J. L. (2000) Interactions of the HIV-1 fusion peptide with large unilamellar vesicles and monolayers. A cryo-TEM and spectroscopic study. *Biochim. Biophys. Acta 1467*, 153−164.

(4) Han, X., Bushweller, J. H., Cafiso, D. S., and Tamm, L. K. (2001) Membrane structure and fusion-triggering conformational change of the fusion domain from influenza hemagglutinin. *Nat. Struct. Biol. 8*, 715−720.

(5) Huster, D., Yao, X. L., and Hong, M. (2002) Membrane protein topology probed by H-1 spin diffusion from lipids using solid-state NMR spectroscopy. *J. Am. Chem. Soc. 124*, 874−883.

(6) Gallagher, G. J., Hong, M., and Thompson, L. K. (2004) Solid-state NMR spin diffusion for measurement of membrane-bound peptide structure: Gramicidin A. *Biochemistry 43*, 7899−7906.

(7) Doherty, T., Waring, A., and Hong, M. (2006) Membrane-bound conformation and topology of the antimicrobial peptide tachyplesin I by solid-state NMR. *Biochemistry 45*, 13323−13330.

(8) Kyrychenko, A., Freites, J. A., He, J., Tobias, D. J., Wimley, W. C., and Ladokhin, A. S. (2014) Structural plasticity in the topology of the membrane-interacting domain of HIV-1 gp41. *Biophys. J. 106*, 610−620.

(9) Toke, O., Maloy, W. L., Kim, S. J., Blazyk, J., and Schaefer, J. (2004) Secondary structure and lipid contact of a peptide antibiotic in phospholipid bilayers by REDOR. *Biophys. J. 87*, 662−674.

(10) Hirsh, D. J., Lazaro, N., Wright, L. R., Boggs, J. M., McIntosh, T. J., Schaefer, J., and Blazyk, J. (1998) A new monofluorinated phosphatidylcholine forms interdigitated bilayers. *Biophys. J. 75*, 1858−1868.

DOI: 10.1021/bi501211x
Biochemistry 2015, 54, 677−684

(11) Schmidt, A., McKay, R. A., and Schaefer, J. (1992) Internuclear distance measurement between Deuterium (I = 1) and a spin-1/2 nucleus in rotating solids. *J. Magn. Reson. 96*, 644−650.
(12) Sack, I., Balazs, Y. S., Rahimipour, S., and Vega, S. (2000) Solid-state NMR determination of peptide torsion angles: Applications of ^{2}H-dephased REDOR. *J. Am. Chem. Soc. 122*, 12263−12269.
(13) Gullion, T., Kishore, R., and Asakura, T. (2003) Determining dihedral angles and local structure in silk peptide by ^{13}C-^{2}H REDOR. *J. Am. Chem. Soc. 125*, 7510−7511.
(14) Xie, L., Ghosh, U., Schmick, S. D., and Weliky, D. P. (2013) Residue-specific membrane location of peptides and proteins using specifically and extensively deuterated lipids and ^{13}C-^{2}H rotational-echo double-resonance solid-state NMR. *J. Biomol. NMR 55*, 11−17.
(15) Cady, S. D., Schmidt-Rohr, K., Wang, J., Soto, C. S., DeGrado, W. F., and Hong, M. (2010) Structure of the amantadine binding site of influenza M2 proton channels in lipid bilayers. *Nature 463*, 689−693.
(16) Long, H. W., and Tycko, R. (1998) Biopolymer conformational distributions from solid-state NMR: α-Helix and 3(10)-helix contents of a helical peptide. *J. Am. Chem. Soc. 120*, 7039−7048.
(17) Zheng, Z., Yang, R., Bodner, M. L., and Weliky, D. P. (2006) Conformational flexibility and strand arrangements of the membrane-associated HIV fusion peptide trimer probed by solid-state NMR spectroscopy. *Biochemistry 45*, 12960−12975.
(18) de Planque, M. R. R., Goormaghtigh, E., Greathouse, D. V., Koeppe, R. E., Kruijtzer, J. A. W., Liskamp, R. M. J., de Kruijff, B., and Killian, J. A. (2001) Sensitivity of single membrane-spanning α-helical peptides to hydrophobic mismatch with a lipid bilayer: Effects on backbone structure, orientation, and extent of membrane incorporation. *Biochemistry 40*, 5000−5010.
(19) Qiang, W., Bodner, M. L., and Weliky, D. P. (2008) Solid-state NMR spectroscopy of human immunodeficiency virus fusion peptides associated with host-cell-like membranes: 2D correlation spectra and distance measurements support a fully extended conformation and models for specific antiparallel strand registries. *J. Am. Chem. Soc. 130*, 5459−5471.
(20) Schmick, S. D., and Weliky, D. P. (2010) Major antiparallel and minor parallel β sheet populations detected in the membrane-associated human immunodeficiency virus fusion peptide. *Biochemistry 49*, 10623−10635.
(21) Brugger, B., Glass, B., Haberkant, P., Leibrecht, I., Wieland, F. T., and Krasslich, H. G. (2006) The HIV lipidome: A raft with an unusual composition. *Proc. Natl. Acad. Sci. U.S.A. 103*, 2641−2646.
(22) Morcombe, C. R., and Zilm, K. W. (2003) Chemical shift referencing in MAS solid state NMR. *J. Magn. Reson. 162*, 479−486.
(23) Bak, M., Rasmussen, J. T., and Nielsen, N. C. (2000) SIMPSON: A general simulation program for solid-state NMR spectroscopy. *J. Magn. Reson. 147*, 296−330.
(24) Zhang, H. Y., Neal, S., and Wishart, D. S. (2003) RefDB: A database of uniformly referenced protein chemical shifts. *J. Biomol. NMR 25*, 173−195.
(25) Tristram-Nagle, S., and Nagle, J. F. (2004) Lipid bilayers: Thermodynamics, structure, fluctuations, and interactions. *Chem. Phys. Lipids 127*, 3−14.
(26) Strandberg, E., Morein, S., Rijkers, D. T. S., Liskamp, R. M. J., van der Wel, P. C. A., and Killian, J. A. (2002) Lipid dependence of membrane anchoring properties and snorkeling behavior of aromatic and charged residues in transmembrane peptides. *Biochemistry 41*, 7190−7198.
(27) Strandberg, E., and Killian, J. A. (2003) Snorkeling of lysine side chains in transmembrane helices: How easy can it get? *FEBS Lett. 544*, 69−73.
(28) Kandasamy, S. K., and Larson, R. G. (2006) Molecular dynamics simulations of model trans-membrane peptides in lipid bilayers: A systematic investigation of hydrophobic mismatch. *Biophys. J. 90*, 2326−2343.
(29) Cheng, X., Jo, S., Marassi, F. M., and Im, W. (2013) NMR-based simulation studies of Pf1 coat protein in explicit membranes. *Biophys. J. 105*, 691−698.
(30) Sackett, K., Nethercott, M. J., Zheng, Z. X., and Weliky, D. P. (2014) Solid-state NMR spectroscopy of the HIV gp41 membrane fusion protein supports intermolecular antiparallel β sheet fusion peptide structure in the final six-helix bundle state. *J. Mol. Biol. 426*, 1077−1094.
(31) Bloom, M., Evans, E., and Mouritsen, O. G. (1991) Physical properties of the fluid lipid-bilayer component of cell membranes: A perspective. *Q. Rev. Biophys. 24*, 293−397.
(32) McDermott, A. (2009) Structure and dynamics of membrane proteins by magic angle spinning solid-state NMR. *Annu. Rev. Biophys. 38*, 385−403.

DOI: 10.1021/bi501211x
Biochemistry 2015, 54, 677−684

Supporting Information

Multiple Locations of Peptides in the Hydrocarbon Core of Gel-Phase Membranes Revealed by Peptide ^{13}C to Lipid ^{2}H REDOR Solid-State NMR

Li Xie, Lihui Jia, Shuang Liang, and David P. Weliky

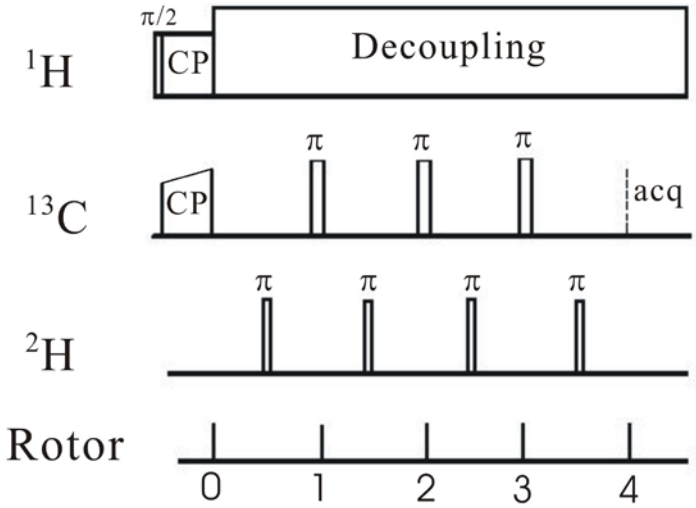

Figure S1. REDOR pulse sequence

1. ^{2}H spectra

Fig. S2 displays the ^{2}H spectra of static (non-spinning) samples obtained with the quadrupolar echo pulse sequence, $(\pi/2)_x$–τ_2–$(\pi/2)_y$–τ_3–detect. Typical experimental parameters included: pulse length ≈ 2 μs; τ_2, τ_3 ≈ 50 μs; and cooling gas temperature of –50 ^{o}C. All spectra had a Pake doublet with $\Delta\nu_Q$ ≈120 kHz that is assigned to –CD_2. The D10 and D54 samples had an additional doublet with $\Delta\nu_Q$ ≈30 kHz that is assigned to –CD_3.

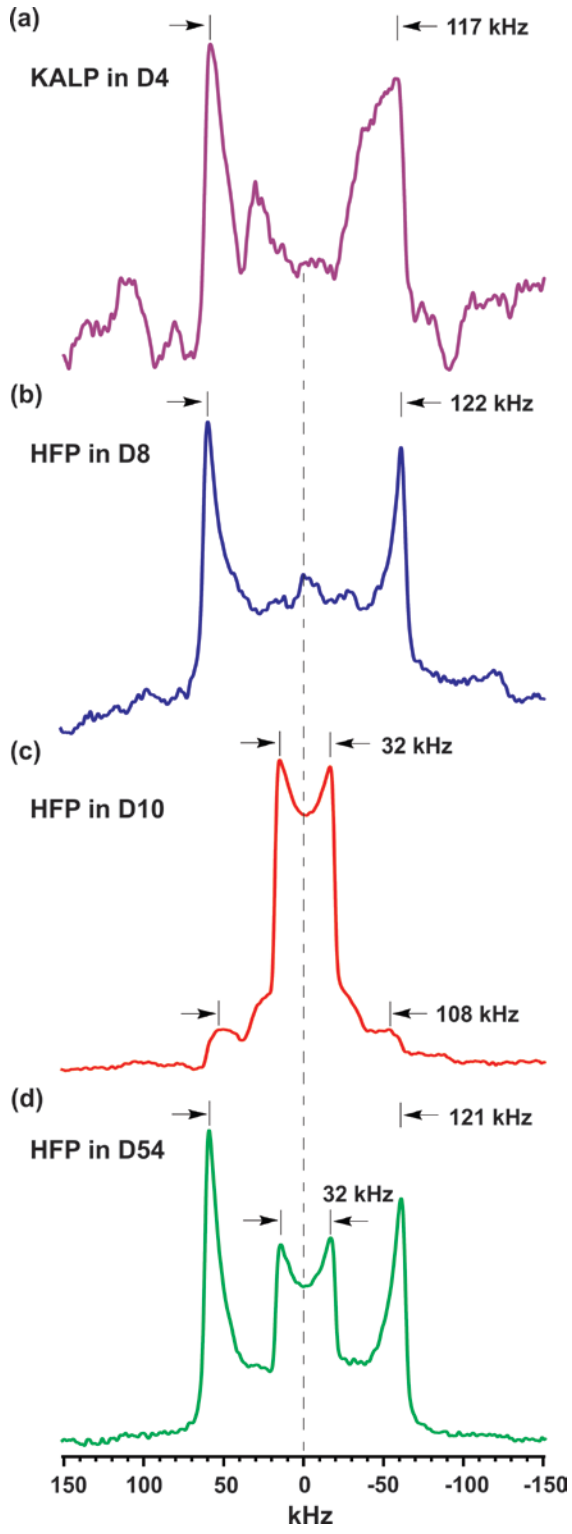

Figure S2. ^{2}H quadrupolar echo spectra

2. SIMPSON simulations

(A) Variation of $\Delta\nu_Q$ with fixed ^{2}H B_1 field = 98 kHz (experimental value)

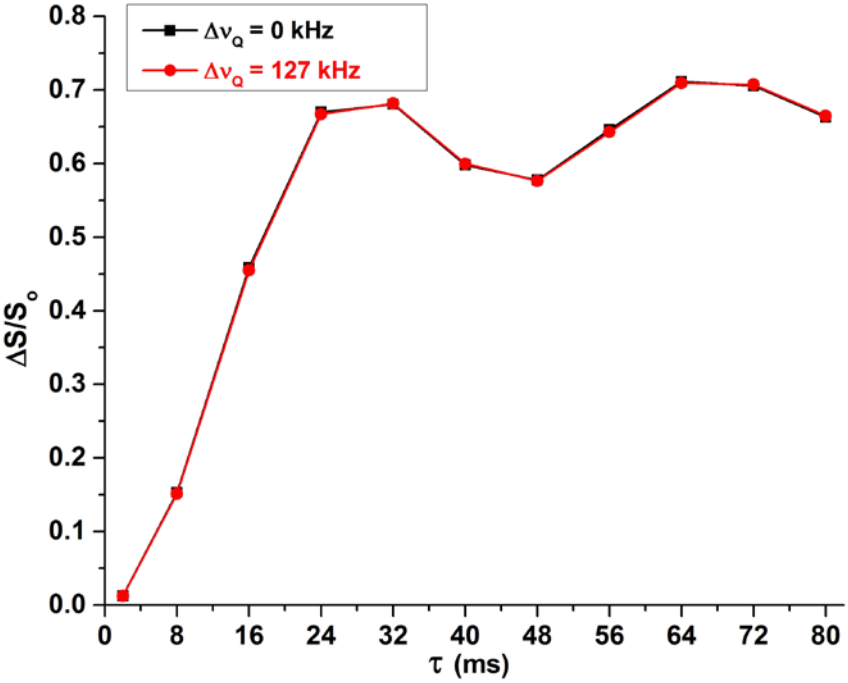

(B) Variation of ^{2}H B_1 field with fixed $\Delta\nu_Q$=127 kHz (rigid C–D value)

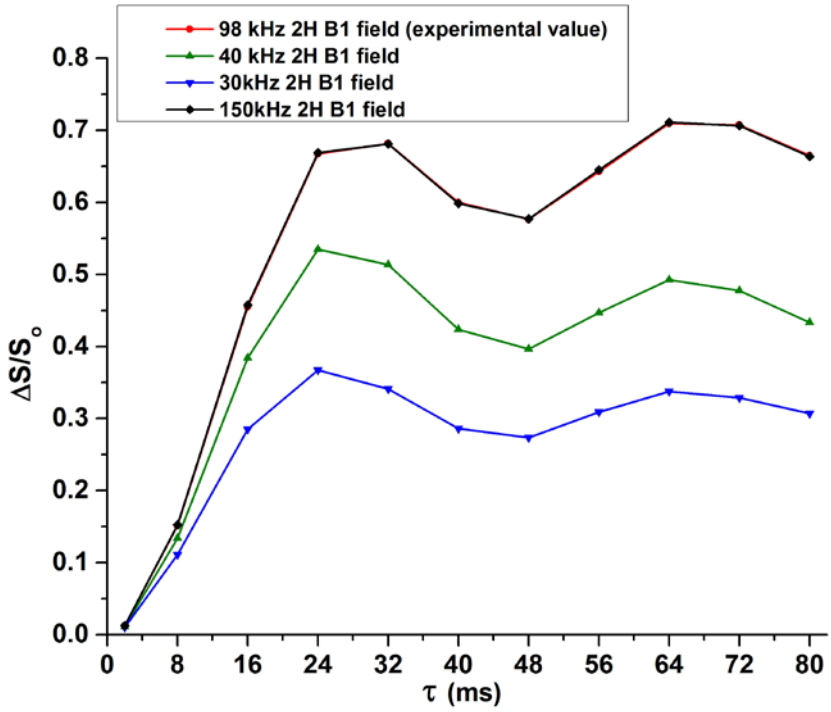

Figure S3. SIMPSON-calculated REDOR buildups of isolated ^{13}C-^{2}H spin pairs with r = 5.0 Å and d = 37 Hz that correspond to their values in the I4 sample. Simulation parameters such as MAS frequency and pulse rf fields were the same as their respective experimental values. Panel A shows that for fixed 98 kHz ^{2}H B_1 field (experimental value), the buildup does not depend on the value of $\Delta\nu_Q$. Panel B shows that for fixed $\Delta\nu_Q$=127 kHz (rigid C–D value), identical buildups are calculated for 98 kHz (experimental value) and 150 kHz ^{2}H B_1 fields. Smaller buildups are observed for 40 and 30 kHz fields that are comparable to those used in earlier ^{13}C-^{2}H REDOR studies (e.g. Ref. 15 in the manuscript).

3. Lipid ^{2}H T_1 determination

Table S1: Best-fit lipid ^{2}H T_1 (ms)

Sample	Static	10 kHz MAS
D54 + HFP	CD_3: 57(2) CD_2: 91(6)	90(4)
D10 + HFP	CD_3: 43(1) CD_2: not determined	CD_3: 58(3) CD_2: 92(8)
D8 + HFP	CD_2: 148(9)	CD_2: 153(3)

The T_1 relaxation times of lipid ^{2}H in HFP_F8$_C$ samples were determined under both static conditions and 10 kHz MAS (Table S1). The pulse sequence was inversion-recovery followed by a quadrupolar-echo, $\pi - \tau_1 - (\pi/2)_x - \tau_2 - (\pi/2)_y - \tau_3 -$ detect. Spectra were acquired for different τ_1 with fixed τ_2 and τ_3. The spectral echo intensity was typically fitted well by:

$$I(\tau_1) = I_0 + \{\Delta I \times [1 - \exp(-\tau_1/T_1)]\}$$

where I_0, ΔI, and T_1 are fitting parameters and respectively correspond to $I(\tau = 0)$, $[I(\tau = \infty) - I(\tau = 0)]$, and 1/(longitudinal ^{2}H relaxation rate). For the D10 sample under MAS, separate $-CD_2$ and $-CD_3$ contributions to $I(\tau_1)$ were considered with distinct $T_{1(CD2)}$ and $T_{1(CD3)}$:

$$I(\tau_1) = I_0 + \{0.4 \times \Delta I \times [1 - \exp(-\tau_1/T_{1(CD2)})]\} + \{0.6 \times \Delta I \times [1 - \exp(-\tau_1/T_{1(CD3)})]\}$$

For a MAS spectrum, the $I(\tau_1)$ was the sum of integrated centerband and sideband intensities. For a static spectrum, individual $I_{CD2}(\tau_1)$ and $I_{CD3}(\tau_1)$ were typically measured because the $-CD_2$ and $-CD_3$ Pake doublets were resolved and separately integrated.

4. REDOR buildups of other samples

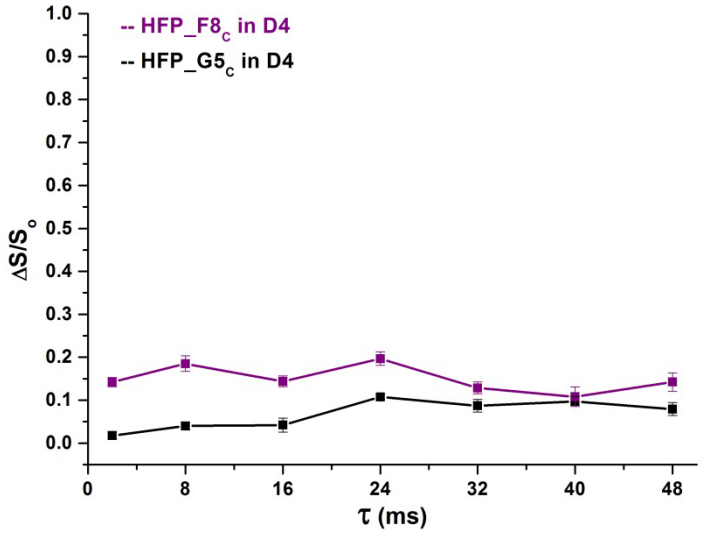

Figure S4. Experimental ($\Delta S/S_0$) of HFP + D4 samples. For HFP_G5$_C$, the ($\Delta S/S_0$) ≤ 0.1 for all τ which is consistent with $r \geq 9$ Å. This limit is based on an expected ($\Delta S/S_0$) of ~0.2 for $r = 9$ Å and τ = 48 ms. For HFP_F8$_C$, the ($\Delta S/S_0$) ≈ 0.15 for all τ and is attributed to the contribution of the natural abundance lipid ^{13}CO nuclei for which $r \approx 2$ Å (Fig. S1B). The F8 ^{13}CO nuclei likely have $r \geq 9$ Å because there is no buildup of ($\Delta S/S_0$) with τ. The HFP_G5$_C$ ($\Delta S/S_0$) do not have a lipid contribution because the lipid and G5 ^{13}CO signals are resolved.

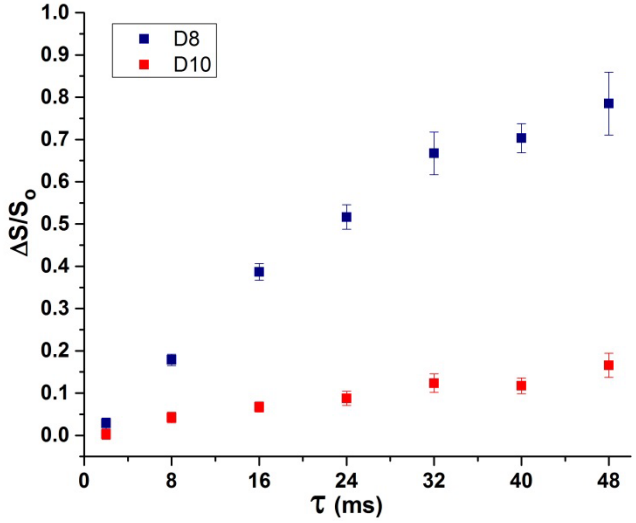

Figure S5. Experimental ($\Delta S/S_0$) of the influenza virus fusion peptide in the D8 (blue) and D10 (red) membrane. The peptide had sequence GLFGAIAGFIENGWEGMIDGGGKKKK and contained a single L2 ^{13}CO label.

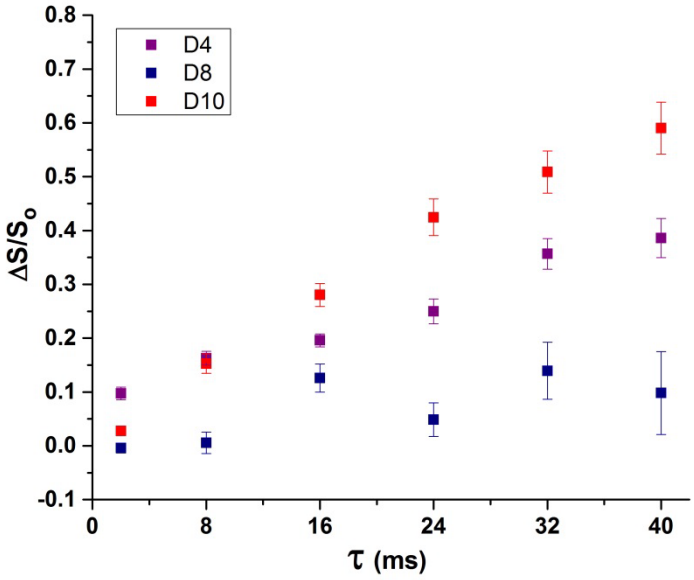

Figure S6. Experimental ($\Delta S/S_0$) of the L9R mutant of HFP_G5$_C$ in the D4 (purple), D8 (blue), and D10 (red) membranes.

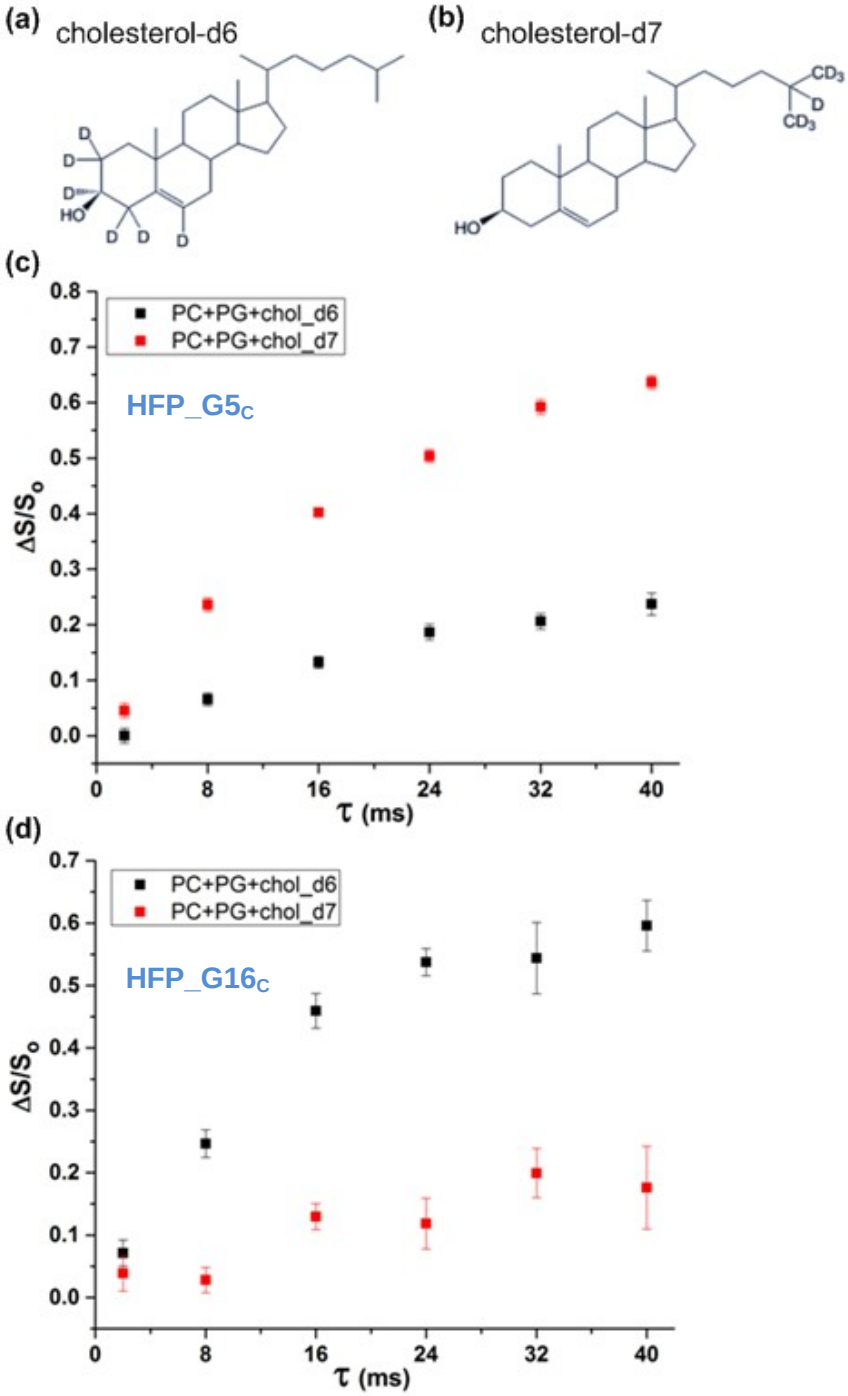

Figure S7. (a, b) Structures of cholesterol-d6 and cholesterol-d7. (c, d) Experimental ($\Delta S/S_0$) of HFP_G5$_C$ and HFP_G16$_C$ in membranes containing (black squares) cholesterol-d6 or (red squares) cholesterol-d7. The membrane composition was PC:PG:cholesterol (8:2:5 mole ratio) and the PC and PG lipids were not deuterated. HFP_G16$_C$ contained a single ^{13}CO label at G16.

5. Models of Membrane Location of KALP

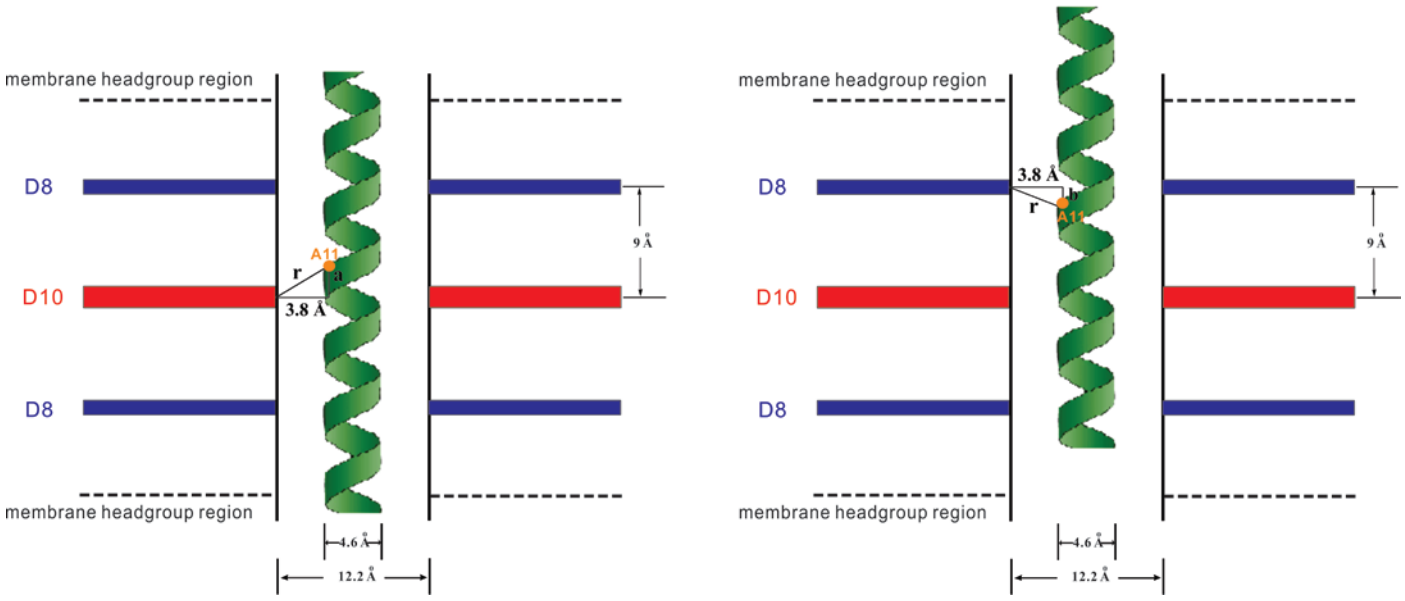

Figure S8. Models of α helical KALP in a DPPC membrane. The green ribbon is the KALP backbone and the vertical lines are the full van der Waals extent of the helix including leucine sidechains. The horizontal black dashed lines are the boundaries of the ~31 Å-thick palmitoyl region of the bilayer. The blue and red bands are the ^{2}H locations of the D8 and D10 membranes, respectively. The left model is the major KALP location with a = 2.4 Å calculated using the best-fit r (D10) = 4.5 Å. The right model is the minor location with (9 Å – b) = 7.8 Å calculated using the best-fit r (D8) = 4.0 Å. If r (D54) = 3.3 Å is used for the helix sidechain dimension, a and (9 Å – b) are respectively 3 and 7 Å. For the minor location, the triangle could be inverted so that the A11 ^{13}CO nucleus is 11 Å from the membrane center. However, this possibility is unlikely because two of the lysine sidechains would be located in the membrane hydrocarbon core.

6. Table S2. $(\Delta S/S_0)^{exp}$ and $(\Delta S/S_0)^{lab}$ of the I4_A9$_C$ sample

Dephasing Time (ms)	$(\Delta S/S_0)^{exp}$	$(\Delta S/S_0)^{lab}$
2	0.014(6)	0.005(8)
8	0.115(3)	0.119(4)
16	0.264(4)	0.281(4)
24	0.384(4)	0.410(5)
32	0.464(6)	0.498(7)
40	0.509(4)	0.547(5)
48	0.566(6)	0.615(8)
56	0.597(3)	0.652(4)
64	0.631(4)	0.687(5)
72	0.652(9)	0.706(10)
80	0.679(6)	0.732(7)